

Supporting Information

Carbon core-shell Pt nanoparticle embedded porphyrin Co-MOF derived N-doped porous carbon for the alkaline AEM water electrolyzer application

Mohan Raj Subramaniam,^a Shanmugam Ramakrishnan,^b Saleem Sidra,^a S.C. Karthikeyan,^a Subramanian Vijayapradeep,^a Jian Huang,^b Mohamed Mamlouk,^b Do Hwan Kim,^{a, c} Dong Jin Yoo^{a, d*}

^aGraduate School, Department of Energy Storage/Conversion Engineering (BK21 FOUR), Hydrogen and Fuel Cell Research Center, Jeonbuk National University, 567 Baekje-daero, Deokjin-gu, Jeonju-si, Jeollabuk-do 54896, Republic of Korea

^bSchool of Engineering, Newcastle University, Merz Court, Newcastle Upon Tyne, NE1 7RU United Kingdom

^cDivision of Science Education and Institute of Fusion Science, Jeonbuk National University, 567 Baekje-daero, Deokjin-gu, Jeonju-si, Jeollabuk-do 54896, Republic of Korea

^dDepartment of Life Science, Jeonbuk National University, 567 Baekje-daero, Deokjin-gu, Jeonju-si, Jeollabuk-do 54896, Republic of Korea

*Corresponding author Email ID: djyoo@jbnu.ac.kr

Characterization techniques

The diffraction pattern of the prepared materials was analysed by using PANalytical (X'PERT-PRO Powder), (mode) with Cu K α radiation ($\lambda=0.154$ nm) X-ray diffraction (XRD) spectrometer. The field emission scanning electron microscope (FE-SEM) with energy-dispersive X-ray spectroscopy (EDS), Carl Zeiss, Germany) and high-resolution transmission electron microscope (HR-TEM), JEM-ARM200F, JEOL) were used to analyze the morphology of the prepared electrocatalyst materials. Raman spectrum was recorded by using NANO PHOTON (RAMAN Touch) instruments equipped with a 532 nm helium-neon laser. Pt, and Co loading was evaluated by inductively coupled plasma-optical emission spectroscopy (ICP-OES) with Thermo Fisher Scientific iCAP 7000 series. The chemical state of the materials was observed by an X-ray photoelectron spectrometer (XPS), Axis-Nova, Kratos Inc. The extended X-ray absorption fine structure (EXAFS) and X-ray absorption near edge structure (XANES) measurement at the Pt-k edges were performed by using the Sc-detector (model R-XAS, Rigaku, Japan) with total electron yield detection.

Electrochemical HER measurements

The ~ 3 mg of electrocatalyst with 5% Nafion (30 μL) were mixed in 1:1 isopropyl alcohol/ DI water solution with 1000 μL and sonicated for 60 minutes to generate a homogenous ink. The prepared ink was coated on carbon paper (coated area 1 cm^2) and then dried at 80 $^\circ\text{C}$ overnight in a vacuum oven. The loading of active materials was approximately ~ 3 mg/cm^2 . As a comparative study, a catalyst ink of commercial Pt-C was prepared using a similar procedure and coated on carbon paper. The HER electrochemical performance was investigated by a distinctive three-electrode cell system of catalyst-coated carbon paper used as a working electrode with Ag/AgCl (reference) electrode and graphite rod (counter electrode). The HER polarization curves were recorded at a 1 mV/s fixed scanning rate. Electrochemical impedance spectroscopy (EIS) of prepared electrocatalysts was measured with a frequency range of 0.01

to 10^6 Hz at a potential amplitude of 5 mV. The prepared catalyst's double-layer capacitance (C_{dl}) value was evaluated using the non-Faradic region of the CV curve with a scanning rate of 5 to 25 mV/s. The mid-point of potential was the difference between the anodic and cathodic current densities. The slope of current densities vs. scan rate was double the value of C_{dl} .

Fabrication of AEM water electrolyzer (AEMWE)

For the AEM water electrolyzer analysis, the membrane electrode assembly (MEA) was fabricated with synthesized and outperformed Pt@Co-NPC-800 as a cathodic electrocatalyst and commercial $NiCo_2O_4$ as anode electrocatalyst. The preparation and functionalized of radiation-grafted AEM of low-density polyethylene (LDPE) with vinyl benzyl chloride (VBC) was used according to previous literature¹⁻³.

The anode catalysts $NiCo_2O_4$ were dispersed in tetrahydrofuran (THF) by ultra-sonication, and the Styrene-ethylene-butylene-styrene (SEBS) ionomer and polytetrafluoroethylene (PTFE) was used as a binder to prepare the ink solution. The prepared ink was sprayed (2 mg/cm^2) loading using a spray gun on a titanium fiber felt gas-diffusion electrode (GDL). Similarly, the Pt@Co-NPC-800 (cathode materials) was mixed with SEBS ionomer and PTFE binder in the presence of isopropanol as a solvent. The cathode ink was sprayed on carbon GDL with an optimized platinum loading of $0.2 \text{ mg}_{Pt}/\text{cm}^2$. After preparing the respective GDLs, the anode and cathode catalysts were soaked with trimethyl amine (TMA) for one day. Here, the prepared electrodes were washed with water several times and dried out properly. Specifically, the anode, cathode, and membrane components were treated with 1M KOH before forming the MEA. Finally, the MEA was kept in a water electrolyzer cell assembly and was torqued to 1.2 Nm. The electrolyzer cell was fed with 1.0 M and 0.1M KOH electrolyte solutions with a 50 mL/min flow rate, and the measurements were recorded.

Electrochemical analysis AEMWE

The linear sweep voltammetry (LSV) was recorded from 1.2 to 2.5 V with a scan rate of 1 mV s⁻¹, and electrochemical impedance spectroscopy (EIS) was performed from 100 kHz to 100 mHz with an amplitude of (V_{rms}) 10 mV and cell voltage of 1.5 V. All the electrochemical tests were performed on a Gamry interface 5000E potentiostat. The evolved H₂ gas analysis utilized the HIDEN Analytical HPR-20 R&D system. AEM electrolyzer cathode outlet (with a carrier nitrogen gas) was connected to the gas analyzer using nitrogen as the carrier gas. The obtained data confirms the presence of hydrogen and nitrogen gases while the AEM electrolyzer operates at 200 mA cm⁻².

Calculation of ECSA

$$ECSA = \frac{C_{dl}}{C_s} \quad (S1)$$

ECSA = Electrochemical active surface area (ECSA)

C_{dl} = Double layer capacitance

C_s = Specific capacitance (0.040 mF cm⁻²)

Calculation of TOF for HER

The hydrogen TOF per site of the Co-NPC-800, Pt@Co-NPC-600 and Pt@Co-NPC-800 catalyst was calculated using following formula (S2):

$$TOF \text{ per site} = \frac{\# \text{ total hydrogen turnover/cm}^2 \text{ geometric area}}{\# \text{ active sites/cm}^2 \text{ geometric area}} \quad (S2)$$

The total number of hydrogens turn overs was calculated by using following formula (S3).

$$\# H_2 = \left(j \frac{mA}{cm^2} \right) \left(\frac{1C}{1000 mA} \right) \left(\frac{1mol e^-}{96485 C} \right) \left(\frac{1mol H_2}{2 mol e^-} \right) \left(\frac{6.02 \times 10^{23} mol H_2}{1 mol H_2} \right) 3.12 \times 10^{15} \frac{s}{cm^2} \text{ per } \frac{mA}{cm^2} \quad (S3)$$

Further Pt and Co content of Pt@Co-NPC-800 catalyst was quantified by using ICP-OES analysis was about ~6.3 and 12.1 % accordingly, the density of active sites based on the Pt and Co is:

$$\left(\frac{6.3}{195.084} + \frac{12.1}{58.93} \right) \times \frac{1mmol}{100 mg} \times 3 \frac{mg}{cm^2} \times 6.022 \times 10^{20} \frac{sites}{mmol} = 4.293 \times 10^{18} sites cm^{-2}$$

For example, TOF of the catalyst at an overpotential of 165 mV was calculated and given below,

$$TOF = \frac{150.6 \times 3.12 \times 10^{15} \frac{H_2}{cm^2 s}}{4.293 \times 10^{18} \text{sites cm}^{-2}} = 0.1095 \text{ s}^{-1}$$

Computational Methodology

Density functional theory (DFT) calculations using the Vienna ab initio simulation package (VASP) were performed to understand the electrocatalytic performance of Co, Pt, and Pt@Co, at different active sites for the hydrogen evolution reaction (HER). The materials were optimized entirely for a stable structure and their formation energy (E_F) was calculated using this formula.

$$E_F = E^* - \sum n_i E_i \quad (S4)$$

In this equation, E^* , n_i , and E_i represent the total energy of the crystal system, the total number of atoms in the crystal structure, and the energy of each individual element, respectively. The generalized gradient approximation (GGA) in the form of Perdew-Burke-Ernzerhof (PBE) functional was employed to approximate the exchange-correlation energy of electrons. The projector augmented wave (PAW) method described the electron-ion interactions. The cut-off energy for the plane-wave basis set was fixed at 400 eV. The DFT-D3, a semiclassical dispersion correction scheme, was employed to describe the effect of the long-range van der Waals interactions. A vacuum space of more than 15 Å was used to avoid interactions between adjacent slabs. The structures were relaxed until the Hellman-Feynman forces were lower than 0.02 eV/Å. Γ -point-centered Monkhorst-Pack meshes of 7 x 7x 1 were applied for the Brillouin zone integrations in DOS calculations. The adsorption of H-atoms on the surfaces of Co (111), Pt (111), and Pt@Co (111) were calculated to obtain the stable configuration for the hydrogen

evolution reaction⁴. The hydrogen adsorption energy (ΔE_{H^*}) was calculated using the formula provided in eq (S4).

$$\Delta E_{H^*} = E_{H^*} - E^* - 1/2E_{H_2} \quad (S5)$$

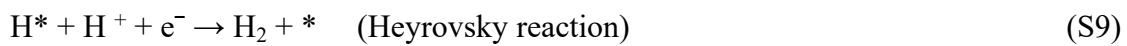
Here, “*” indicates active sites of electrocatalytic materials. E_{H^*} , E^* , and, E_{H_2} represent total energy of material with and without H-atom adsorption and the energy of hydrogen molecule (H_2). The Gibbs free energy (ΔG_{H^*}) in HER was calculated using the following formula;

$$\Delta G_{H^*} = \Delta E_{H^*} + \Delta ZPE - T\Delta S \quad (S6)$$

ΔE_{H^*} , ΔZPE , and, $T\Delta S$ are H-atom adsorption energy, zero-point energy, and, room temperature, and change in entropy, respectively. Combining eq (S5) and eq (S6) results in (S7).

$$\Delta G_{H^*} = E_{H^*} - E^* - 1/2E_{H_2} + \Delta ZPE - T\Delta S \quad (S7)$$

The three steps Volmer, Heyrovsky, and, Tafel are responsible for HER, and they are given below.



The catalytic activity in HER can be analyzed by Volmer reaction in eq (S8).

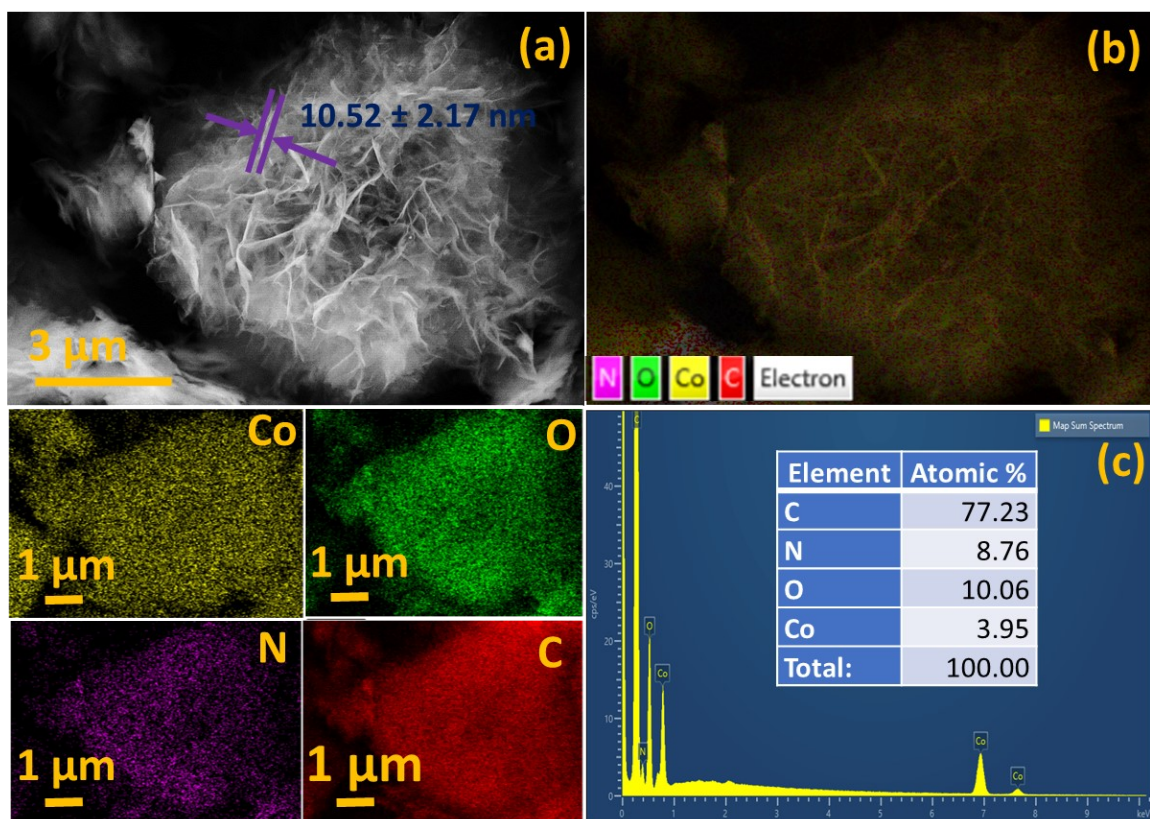


Fig. S1 (a) FE-SEM image of flower like-Co-MOFs, (b) selected area elemental mapping of Co, O, N, and C, and (c) corresponding EDS spectrum.

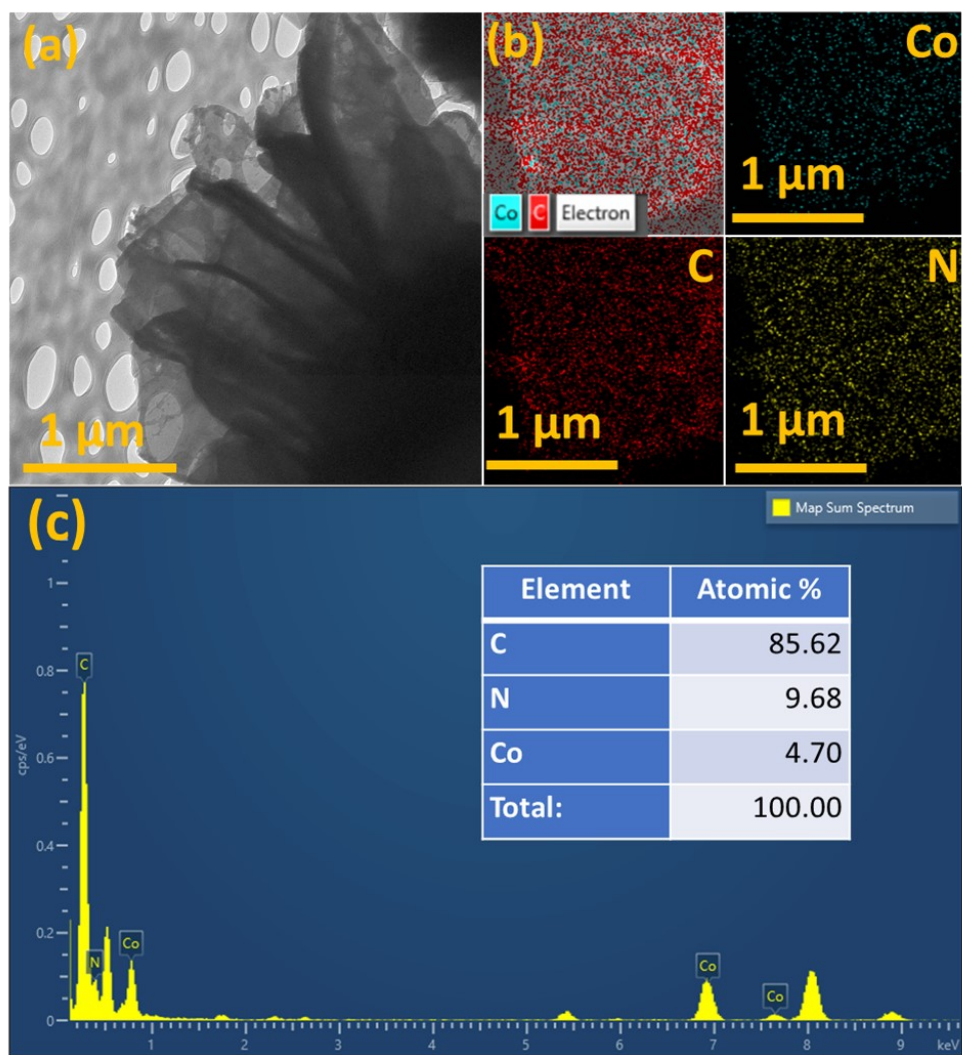


Fig. S2 (a) HR-TEM image of Co-NPC-800, (b) elemental mapping of Co, N, and C, and (c) corresponding EDS spectrum.

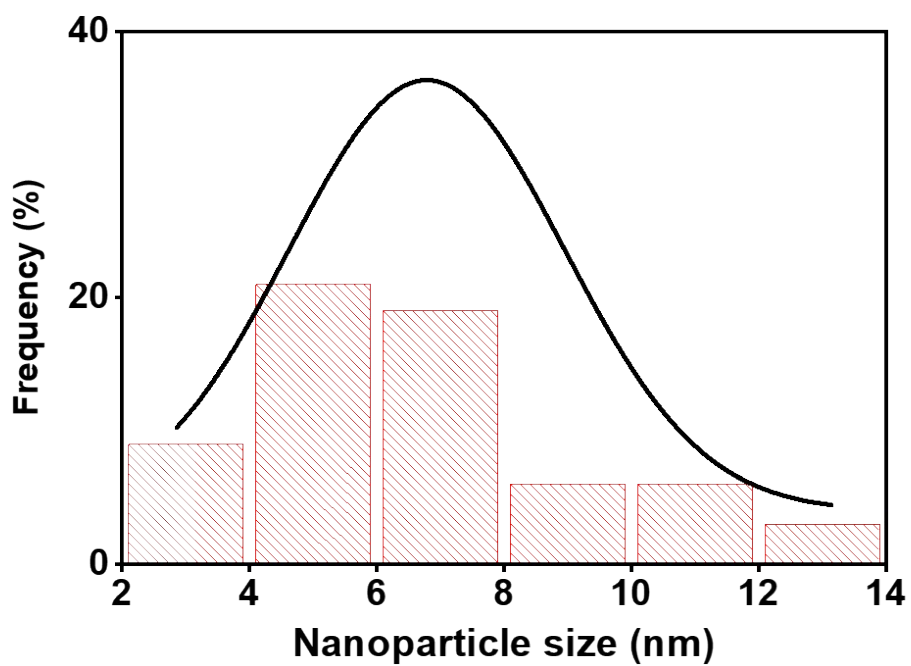


Fig. S3. HR-TEM histogram of Pt@Co nanoparticles in Pt@Co-NPC-800 electrocatalyst

Table S1. Pt@Co-NPC-800 electrocatalyst XPS element composition.

Name	Peak Binding energy	FWHM (eV)	Area (P) CPS. (eV)	Atomic %
Pt 4f	70.59	1.36	79401.43	1.21
C 1s	283.72	1.67	257646.5	74.05
N 1s	397.88	1.73	34552.39	6.39
O 1s	531.14	4.17	125223.3	14.89
Co 2p	779.34	3.59	147429.8	3.46

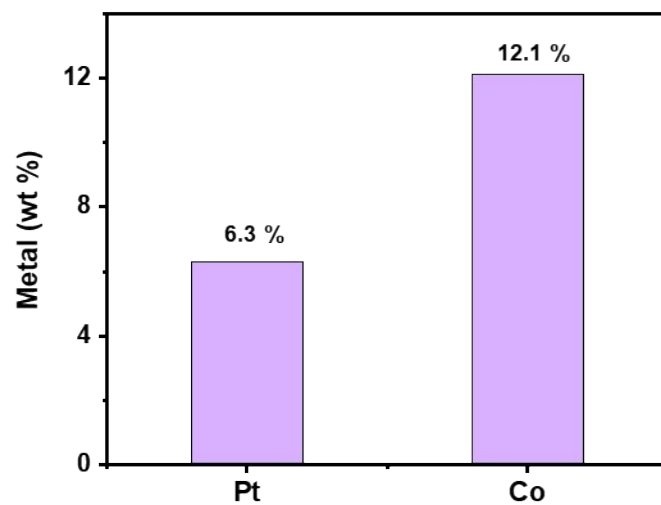


Fig. S4. ICP-OES results of Pt@Co-NPC-800 electrocatalyst.

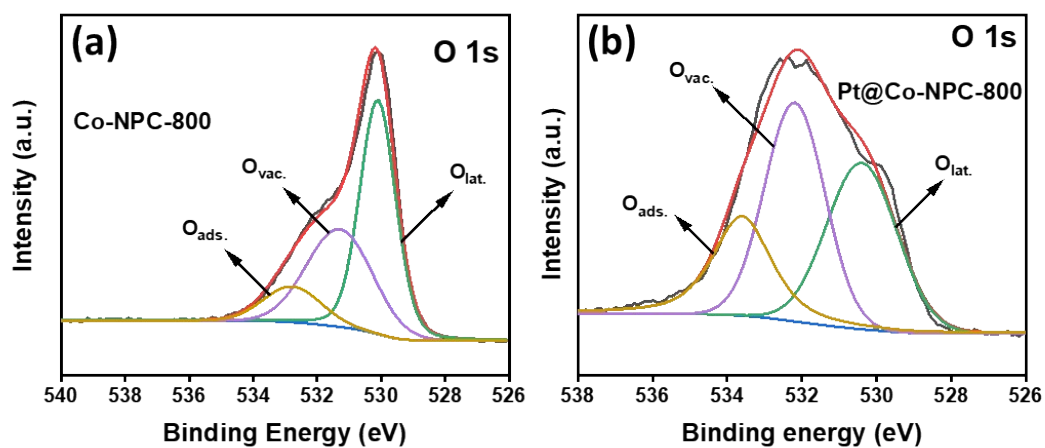


Fig. S5 XPS deconvoluted O 1s spectra of (a) Co-NPC-800 and (b) Pt@Co-NPC-800.

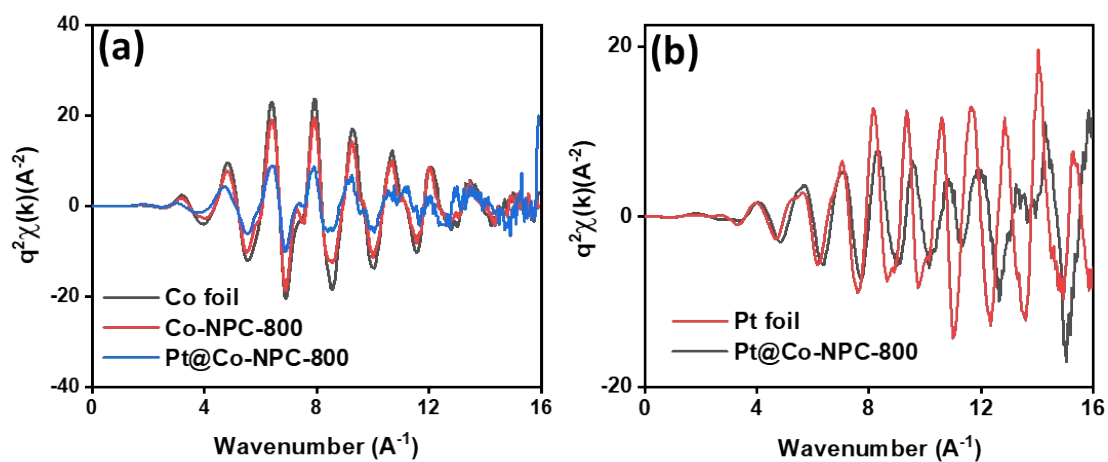


Fig. S6 XAS analysis: fitted K-space values of (a) Co K edge (K₃ weighting) of Co foil, Co-NPC-800 and Pt@Co-NPC-800, and (b) Pt K edge (K₃ weighting) of Pt foil and Pt@Co-NPC-800.

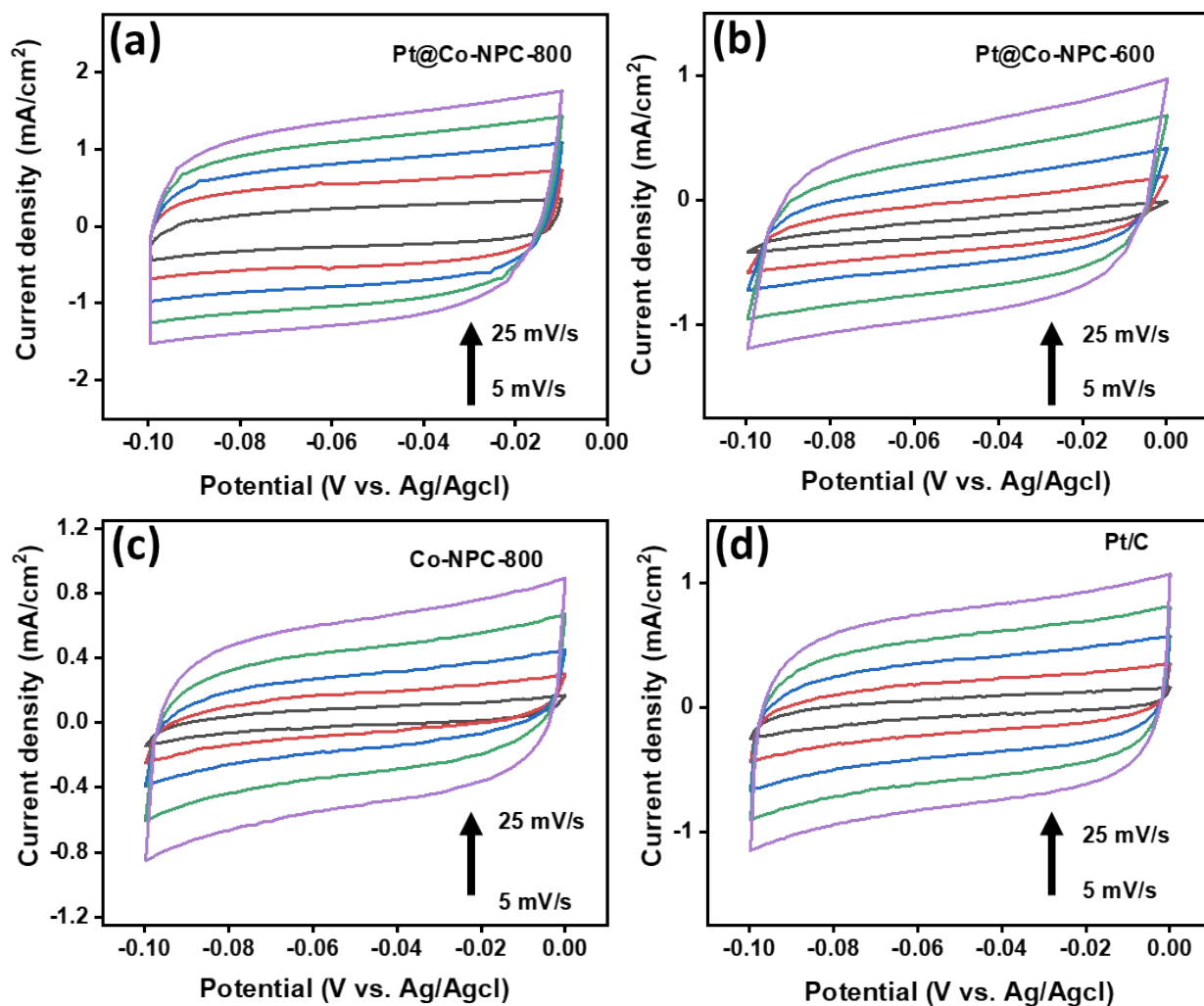


Fig. S7 Double layer capacitance (C_{dl}) calculations (a-d) recorded CV curves at linear incremental scan rates (5-25 mV/s) of Pt@Co-NPC-800, Pt@Co-NPC-600, Co-NPC-800, and commercial Pt/C, respectively.

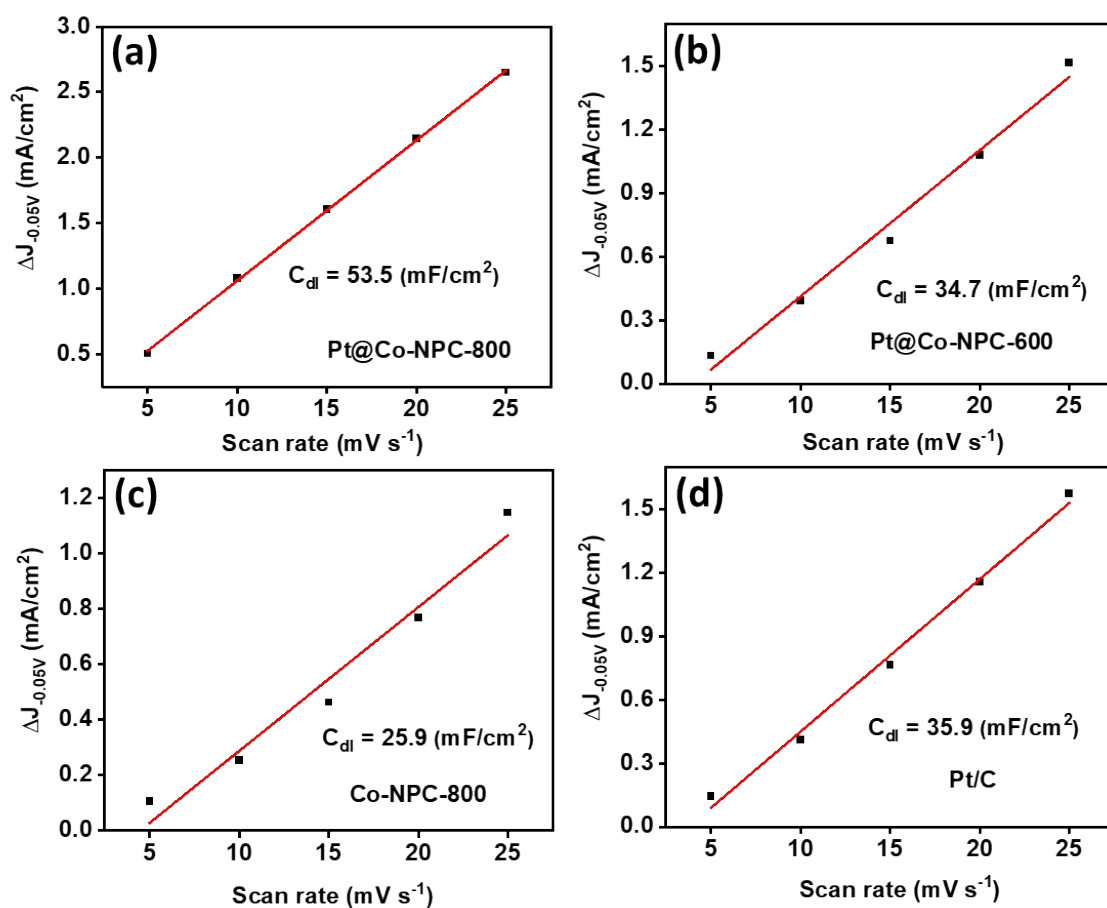


Fig. S8 C_{dl} values at 0.05 V_{RHE} (a) Pt@Co-NPC-800, (b) Pt@Co-NPC-600, (c) Co-NPC-800, and (d) Pt/C.

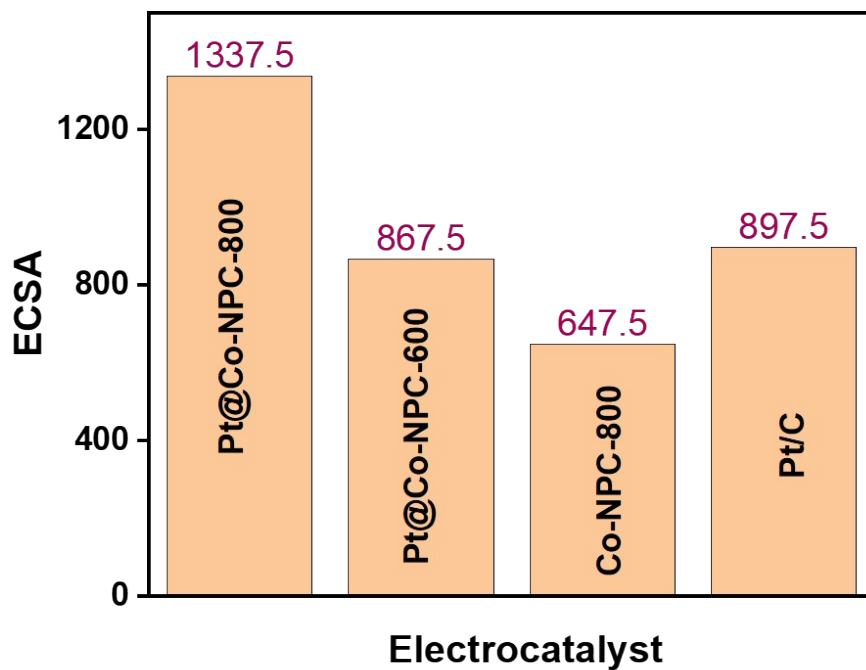


Fig. S9 Comparison chart of calculated ECSA values for Pt@Co-NPC-800, Pt@Co-NPC-600, Co-NPC-800, and Pt/C.

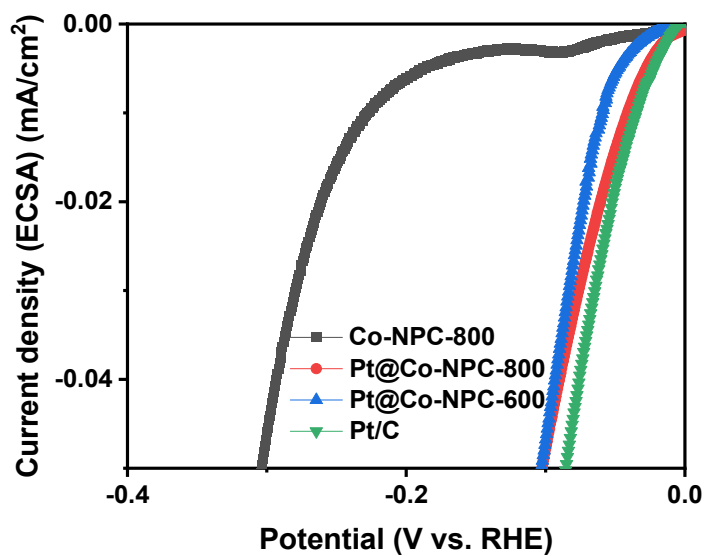


Fig. S10 ECSA normalized LSV curve of Co-NPC-800, Pt@Co-NPC-800, Pt@Co-NPC-600 and Pt/C in 1.0 M KOH.

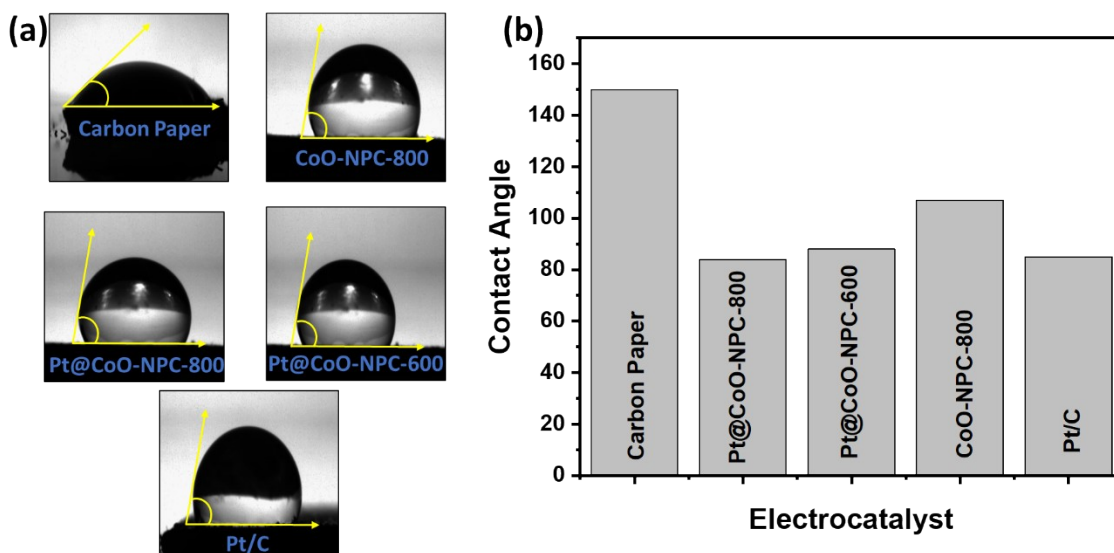


Fig. S11 (a) contact angles measurement of carbon paper, Co-NPC-800, Pt@Co-NPC-800, Pt@Co-NPC-600, and Pt/C in carbon paper, and (b) recorded contact angle values.

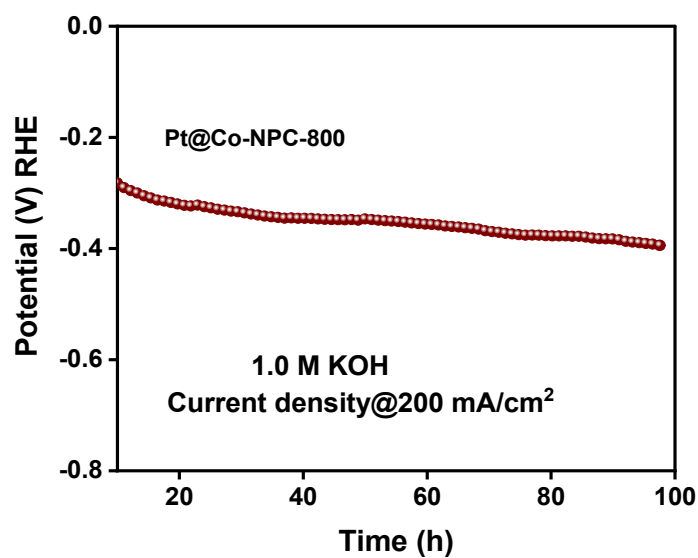


Fig. S12 Chronopotentiometry analysis of Pt/C and Pt@Co-NPC-800 catalysts at 200 mA cm⁻² current density.

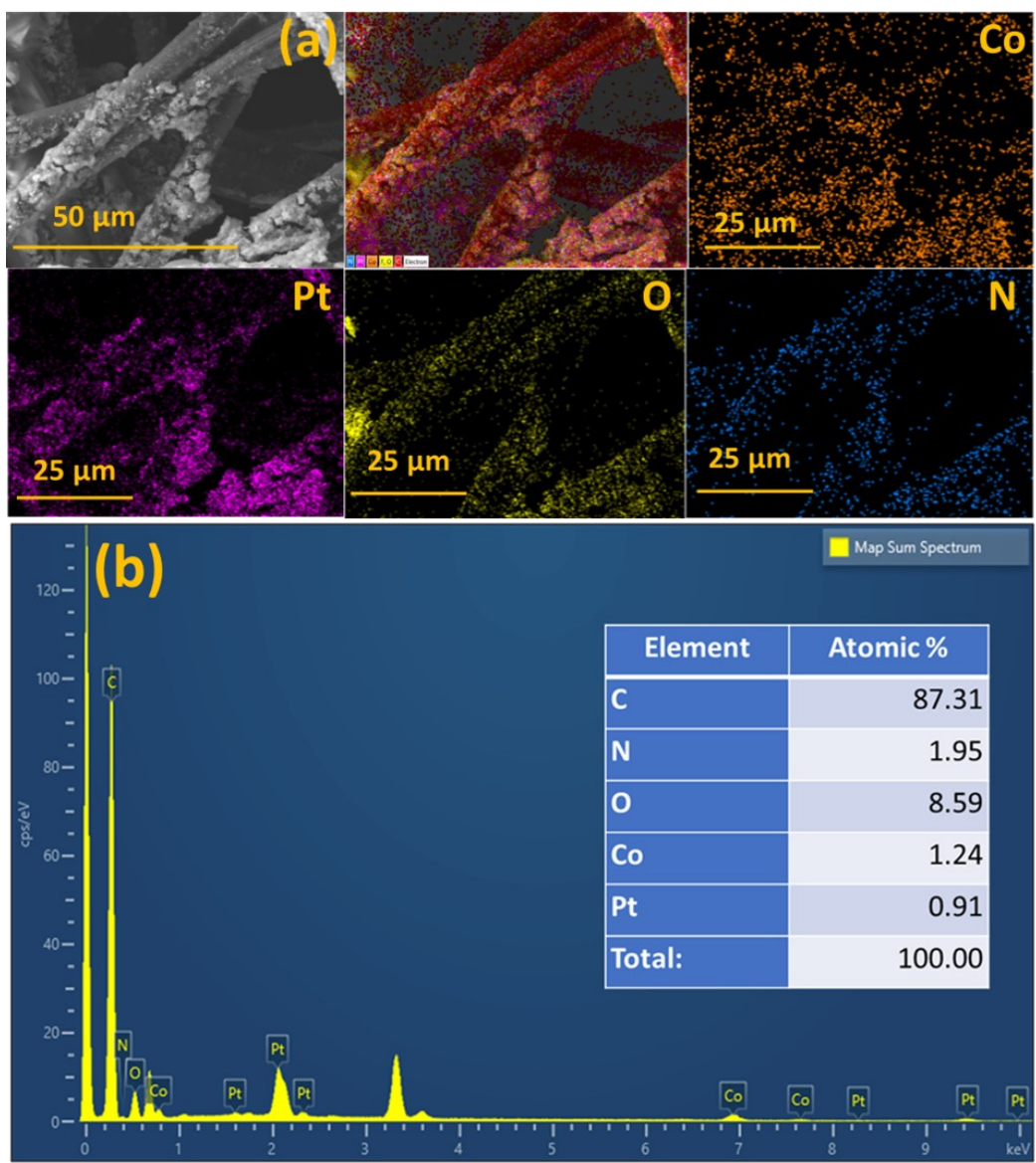


Fig. S13 Post durability morphological FE-SEM investigative results: (a) selective area elemental mapping indicating overall, Co, Pt, O, and N, and (b) corresponding EDS spectrum.

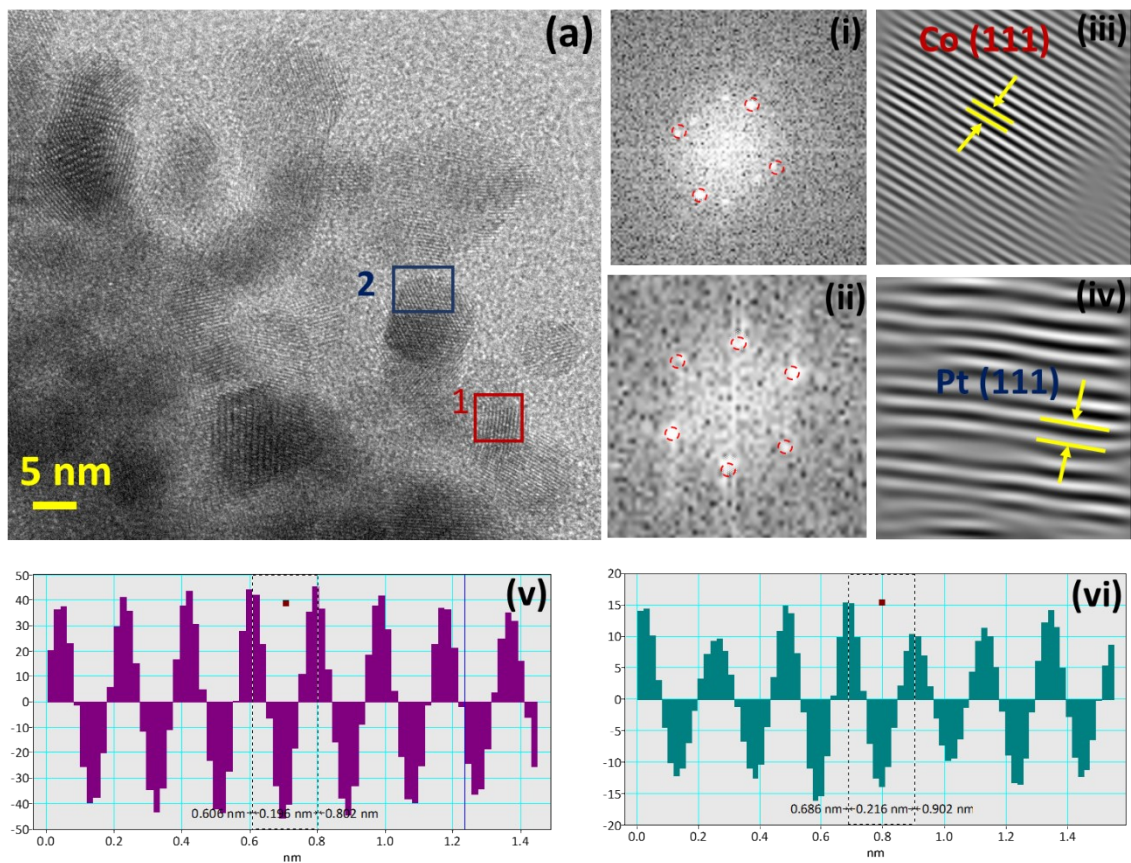


Fig. S14 Post durability morphological HR-TEM investigative results: (a) HR-TEM image, and (i-vi) i-FFT image and spot pattern of Co (111) and Pt (111) plane.

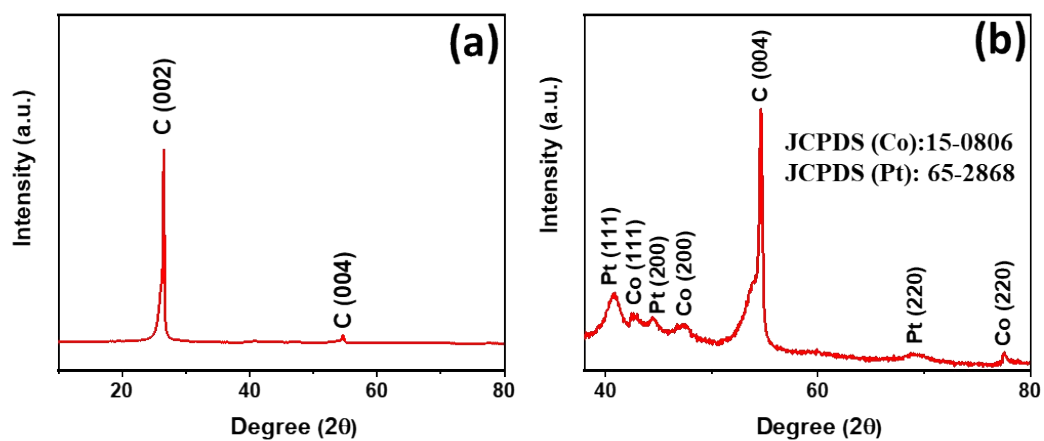


Fig. S15 Post durability XRD investigative results of Pt@Co-NPC-800 carbon paper electrode

(a) XRD pattern and (b) enlarged view of XRD pattern.

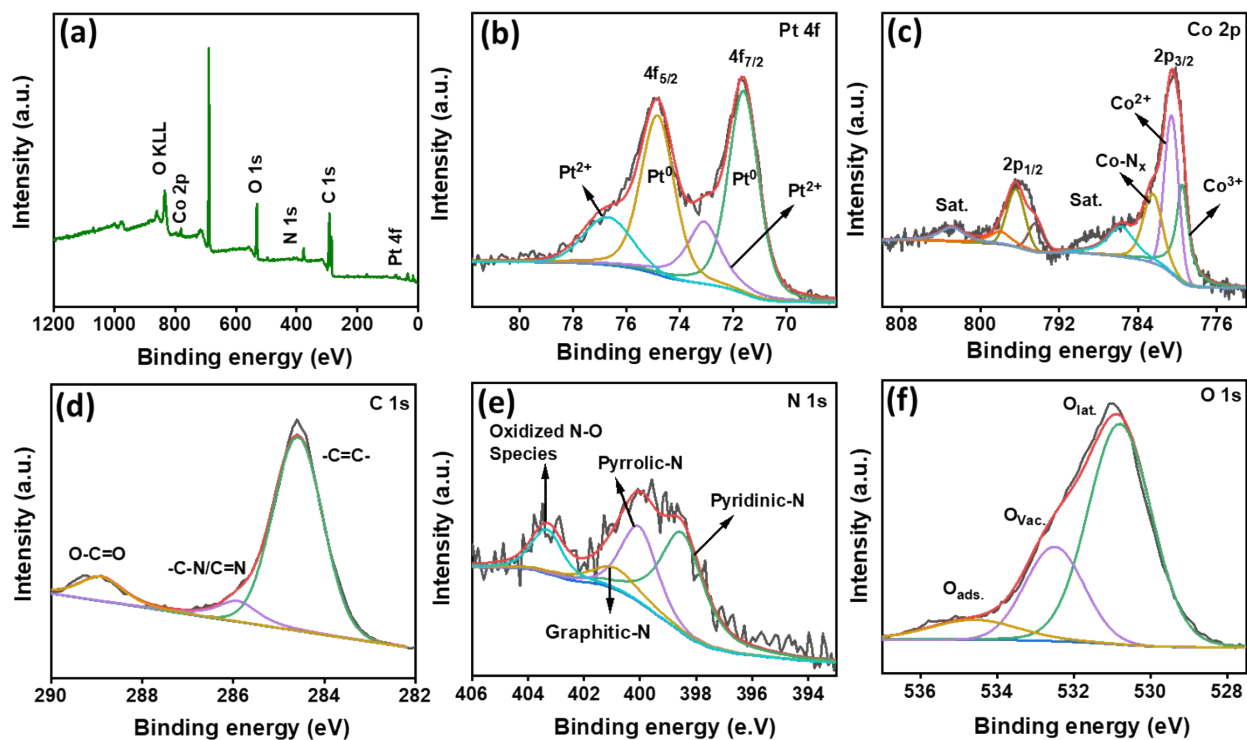


Fig. S16 Post durability XPS investigative results of Pt@Co-NPC-800 (a) Overall XPS survey spectra, Deconvoluted high resolution spectra of (b) Pt 4f, (c) Co 2p, (d) C 1s, (e) N 1s, and (f) O 1s.

Table S2 Comparison of Pt@Co-NPC-800 HER activity with recently reported PtCo with carbon materials-based catalysts.

Electrocatalyst	Electrolyte	Overpotential (mV@10mA/cm²)	Tafel slope (mV/dec¹)	References
Pt@Co-NPC	1.0 M KOH	36	42.7	This work
Co-Pt/C/NAs	1.0 M KOH	50	46	4
PtCo	1.0 M KOH	47.2	50	5
PtCo/NCNT	1.0 M KOH	53	54.1	6
Pt-Ni (OH) ₂	1.0 M KOH	85.5@4 mA/cm ²	-	7
Pt ₃ Ni ₂	1.0 M KOH	70@37.5 mA/cm ²	-	8
Pd@PtCu	1.0 M KOH	60	26.2	9
PtCoCu	1.0 M KOH	48	32.8	10
PtNi/C	1.0 M KOH	39.7	55	11
Pt-NiO	1.0 M KOH	39.8	79.8	12
Co@NPC	1.0 M NaOH	325	117	13
Pt/Nb-Co(OH) ₂	1.0 M KOH	112	82	14
Pt-Ni (OH) ₂	1.0 M KOH	39	55	15
Pt-Ni ₂ Fe	1.0 M KOH	80	67	16
Pt ₂ Ni ₃ -P NWs	1.M KOH	44	66	17

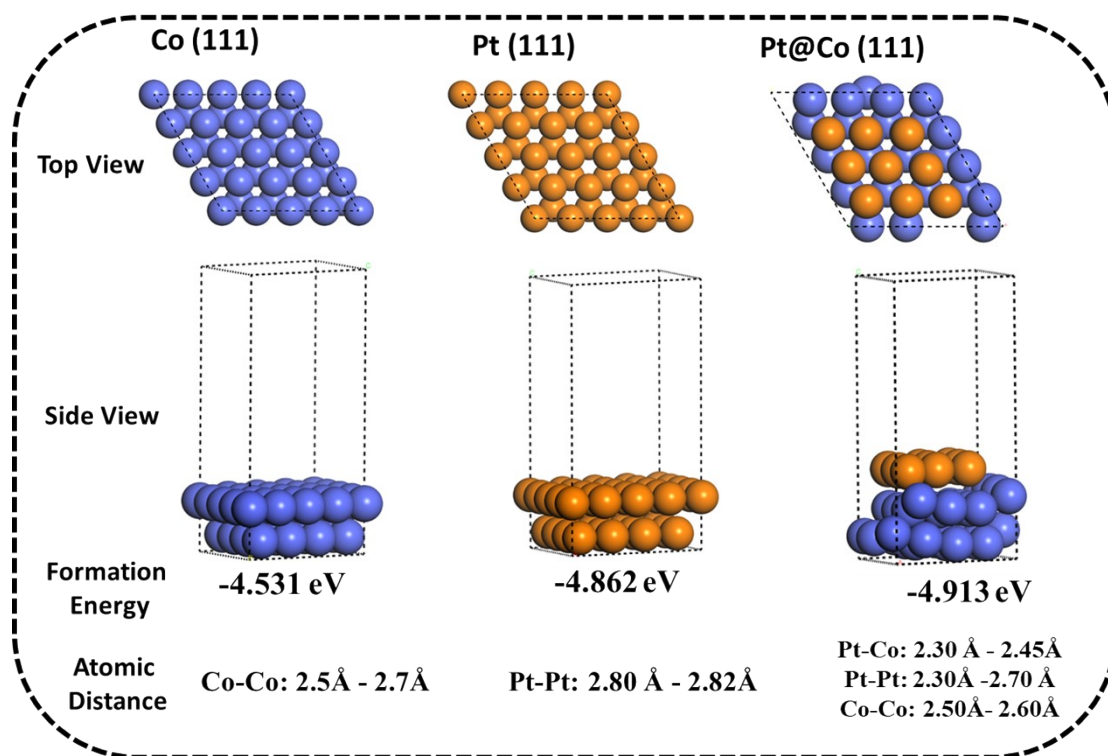


Fig. S17 Top and side views of Co (111), Pt (111), and Pt@Co (111)

Table. S3 Formation energy of Pt (111), Co (111), Pt@Co (111) electrocatalysts

Electrocatalyst	Formation energy (eV)
Co (111)	-4.531
Pt (111)	-4.862
Pt@Co (111)	-4.913

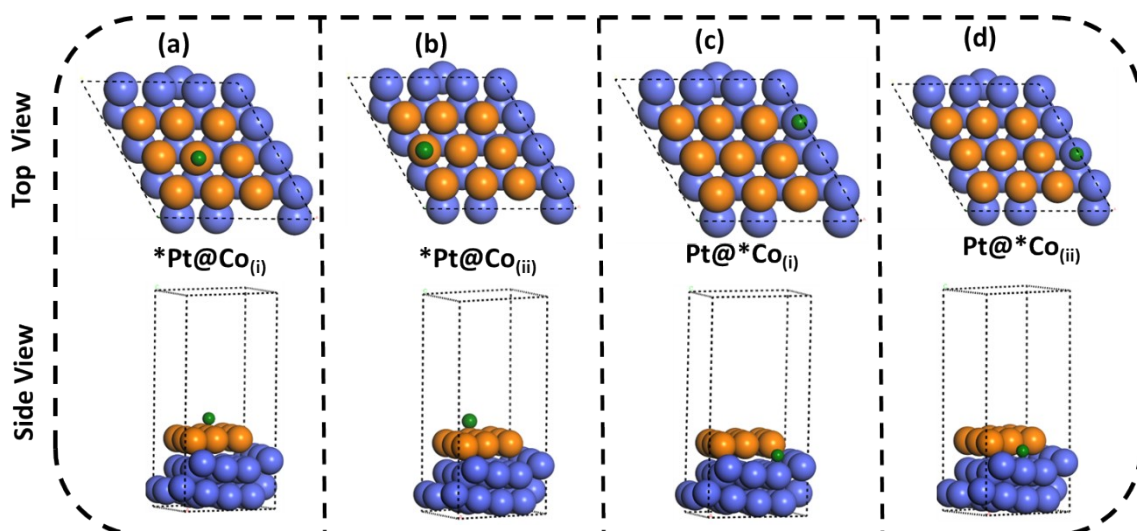


Fig. S18 Top and side views of Pt@Co (111) after H-atom adsorption at (a) 1-Pt, (b) 2-Pt, (c) 1-Co, and (d) 2-Co active-sites.

Table. S4 H-adsorption energy of Pt (111), Co (111), Pt@Co (111) at Pt and Co active sites.

Adsorption Energy (eV)	Adsorption Sites	
	Pt	Co
Co		-0.271
Pt	-0.217	
*Pt@Co _(I)	-0.101	
*Pt@Co _(II)	-0.134	
Pt@*Co _(I)		-0.341
Pt@*Co _(II)		-0.175

Table. S5 Gibbs free energy of H-adsorption on Pt (111), Co (111), Pt@Co (111) at Pt and Co active sites.

Gibbs Free Energy Change (eV)	Adsorption Sites	
	Pt	Co
Co		0.346
Pt	-0.286	
*Pt@Co (I)	-0.120	
*Pt@Co (II)	0.137	
Pt@*Co (I)		-0.316
Pt@*Co (II)		-0.228

References

1. M. Mamlouk, J. A. Horsfall, C. Williams and K. Scott, *Int. J. Hydrog. Energy*, 2012, **37**, 11912-11920.
2. G. Gupta, K. Scott and M. Mamlouk, *J. Power Sources*, 2018, **375**, 387-396.
3. S. Ramakrishnan, S. Vijayapradeep, S. C. Selvaraj, J. Huang, S. C. Karthikeyan, R. Gutru, N. Logeshwaran, T. Miyazaki, M. Mamlouk and D. J. Yoo, *Carbon*, 2024, **220**, 118816.
4. H. Zhang, Y. Liu, H. Wu, W. Zhou, Z. Kou, S. J. Pennycook, J. Xie, C. Guan and J. Wang, *Journal of Materials Chemistry A*, 2018, **6**, 20214-20223.
5. J. Hu, C. Fang, X. Jiang, D. Zhang and Z. Cui, *Inorganic Chemistry Frontiers*, 2020, **7**, 4377-4386.
6. S. L. Zhang, X. F. Lu, Z.P. Wu, D. Luan and X. W. Lou, *Angewandte Chemie International Edition*, 2021, **60**, 19068-19073.
7. H. Yin, S. Zhao, K. Zhao, A. Muqsit, H. Tang, L. Chang, H. Zhao, Y. Gao and Z. Tang, *Nature Communications*, 2015, **6**, 6430.
8. P. Wang, X. Zhang, J. Zhang, S. Wan, S. Guo, G. Lu, J. Yao and X. Huang, *Nature Communications*, 2017, **8**, 14580.
9. M. Bao, I. S. Amiin, T. Peng, W. Li, S. Liu, Z. Wang, Z. Pu, D. He, Y. Xiong and S. Mu, *ACS Energy Letters*, 2018, **3**, 940-945.
10. Y. Liu, Y. Wang, P. Yang and G. Gao, *International Journal of Hydrogen Energy*, 2021, **46**, 37311-37320.
11. H. Chen, G. Wang, T. Gao, Y. Chen, H. Liao, X. Guo, H. Li, R. Liu, M. Dou, S. Nan and Q. He, *The Journal of Physical Chemistry C*, 2020, **124**, 5036-5045.
12. Z. Zhao, H. Liu, W. Gao, W. Xue, Z. Liu, J. Huang, X. Pan and Y. Huang, *Journal of the American Chemical Society*, 2018, **140**, 9046-9050.

13. K. Nath, K. Bhunia, D. Pradhan and K. Biradha, *Nanoscale Advances*, 2019, **1**, 2293-2302.
14. Y. Tian, M. Wen, A. Huang, Q. Wu, Z. Wang, Q. Zhu, T. Zhou and Y. Fu, *Small*, 2023, **19**, 2207569.
15. X. Yu, J. Zhao, L.R. Zheng, Y. Tong, M. Zhang, G. Xu, C. Li, J. Ma and G. Shi, *ACS Energy Letters*, 2018, **3**, 237-244.
16. L. Wang, L. Zhang, W. Ma, H. Wan, X. Zhang, X. Zhang, S. Jiang, J. Y. Zheng and Z. Zhou, *Advanced Functional Materials*, 2022, **32**, 2203342.
17. P. Wang, Q. Shao, J. Guo, L. Bu and X. Huang, *Chemistry of Materials*, 2020, **32**, 3144-3149.